



Cite this: *Phys. Chem. Chem. Phys.*,
2014, 16, 22462

Received 28th July 2014,
Accepted 3rd September 2014

DOI: 10.1039/c4cp03883e

www.rsc.org/pccp

Photoelectrochemical reduction of aqueous protons with a CuO|CuBi₂O₄ heterojunction under visible light irradiation†

Hyun S. Park, Chong-Yong Lee and Erwin Reisner*

A p-type heterojunction photoelectrode consisting of platinized CuBi₂O₄ layered on a CuO film was prepared. The CuO|CuBi₂O₄|Pt electrode photo-generates H₂ in pH neutral aqueous solution during visible light irradiation and exhibits a substantially enhanced photocurrent compared to CuO|Pt and CuBi₂O₄|Pt electrodes. Reduced electron–hole recombination by the band offsets in the heterostructure is responsible for the improved photoelectrochemical performance of CuO|CuBi₂O₄ with a small band-gap of approximately 1.5 eV.

The development of an efficient, stable, and scalable photocatalyst for the conversion of solar energy into chemical energy is a major goal to address the energy challenge of this century. Photolysis of water into H₂ and O₂ on semiconductors has been studied for decades,¹ and current efforts focus on the discovery of small band-gap photocatalysts with high activity during visible light irradiation.

Theoretically, a band-gap of less than 1.8 eV would allow for a photon-to-H₂ conversion efficiency of more than 20%.^{2,3} A common strategy to achieve high efficiency is pairing a small band-gap photocathode for H₂ production with a semiconductor photoanode with complementary light absorption for water oxidation.^{4,5} Beyond efficiency, the semiconductor electrodes must also be made of inexpensive materials, easy to fabricate and display long-term stability in aqueous electrolyte solution.⁶

Despite a large number of encouraging n-type photoanodes being available,^{7–11} there are only a few promising candidates for efficient p-type photocathodes for the H₂ evolution reaction (HER). Many p-type semiconductors, e.g., p-doped Si,¹² Cu₂O,^{13–15} InP,¹⁶ Cu₂ZnSnS₄,¹⁷ CuIn_xGa_{1–x}Se₂,¹⁸ WSe₂,¹⁹ CuRhO₂,²⁰ CuO,²¹ and CuBi₂O₄,^{22–24} have been discussed for the photoelectrochemical (PEC) HER using solar energy. However, these photocathodes

have currently restricted utility due to their high cost and/or rapid photo-decomposition in aqueous solution.

CuBi₂O₄ is a natural mineral semiconductor with a tetragonal structure, which is (photo-)chemically unstable in acidic and pH neutral aqueous solution.^{23,25} Despite the attractive band-gap size of approximately 1.5 to 1.8 eV of the p-type semiconductor, there is only a limited number of studies where CuBi₂O₄ was employed as a photoelectrocatalyst.^{22–24} CuO is another attractive and promising p-type semiconductor with a small band-gap.^{26,27} It has a conduction band position suitable for HER and has been used as coating on TiO₂ and Cu₂O for visible light absorption and to improve the photochemical stability of the electrode, respectively.^{28,29} However, CuO and CuBi₂O₄ suffer from severe photodegradation in aqueous solution through photoreduction to metallic copper.²³

Herein, we report on the simple preparation of an inexpensive photocathode based on a CuO|CuBi₂O₄ heterojunction coated with Pt for visible light promoted HER in pH neutral aqueous electrolyte solution (Fig. 1). The enhanced photocurrent is the result of improved electron–hole separation by utilizing the valence band offsets at the heterojunction interface and the Pt-layer enhanced the photostability of the CuO|CuBi₂O₄ heterojunction.

CuO, CuBi₂O₄ and CuO|CuBi₂O₄ thin film electrodes were prepared by drop-casting the precursor solution (Cu(NO₃)₂ and

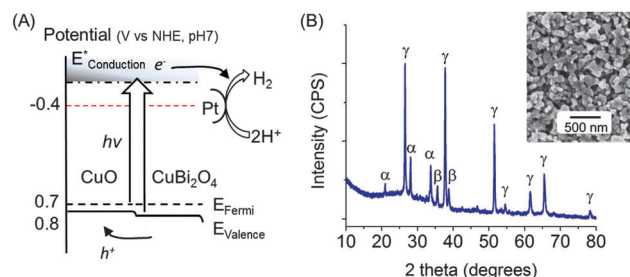


Fig. 1 (A) Schematic energy diagram of the estimated band-edge positions of CuO|CuBi₂O₄|Pt heterojunction. (B) Powder X-ray diffraction patterns of CuO|CuBi₂O₄ heterojunction (α = CuBi₂O₄, PDF#48-1886; β = CuO, PDF#44-0706; and γ = FTO). Inset in (B) shows an SEM image of CuO|CuBi₂O₄ electrode surface.

Christian Doppler Laboratory for Sustainable SynGas Chemistry,
Department of Chemistry, University of Cambridge, Lensfield Road,
Cambridge CB2 1EW, UK. E-mail: reisner@ch.cam.ac.uk

† Electronic supplementary information (ESI) available: Experimental details and additional results including photoelectrochemical measurements and material characterizations of electrodes. See DOI: 10.1039/c4cp03883e



Bi(NO₃)₃ in ethylene glycol) onto fluorine-doped tin oxide (FTO)-coated glass followed by heat treatment at 500 °C in air (see ESI† for Experimental details and characterization). X-ray diffraction patterns show monoclinic CuO (PDF#44-0706) and Kusaichiite tetragonal CuBi₂O₄ (PDF#48-1886) without secondary phase formation in the homo-layered and heterostructured thin film electrodes (Fig. 1 and Fig. S1, ESI†). The crystal size observed by scanning electron microscopy (SEM) was approximately 100 nm for the FTO|CuO and FTO|CuO|CuBi₂O₄ heterojunction films, whereas a smooth surface was observed for the FTO|CuBi₂O₄ film (Fig. 1 and Fig. S2, ESI†). The FTO|CuO|CuBi₂O₄ heterojunction film shows a porous structure similar to that of FTO|CuO with a film thickness of about 300 nm as shown in the cross section image in Fig. S2 (ESI†).

The photoactivity of the Pt-free electrodes was first studied by linear sweep voltammetry (LSV) and chronoamperometry (CA) at 0.2 V vs. normal hydrogen electrode (NHE) in a pH 6.8 aqueous solution (Fig. S3 and S4, ESI†). An AM 1.5G solar light irradiator with a UV-vis light intensity of 100 mW cm⁻² was employed. As expected, FTO|CuO, FTO|CuBi₂O₄, and FTO|CuO|CuBi₂O₄ showed poor photo-stability due to the photo-decomposition of the electrodes during irradiation (Fig. S4, ESI†). The photocurrent onset at FTO|CuBi₂O₄ in LSV runs was observed at approximately 100 mV more positive potential compared to FTO|CuO (Fig. S3, ESI†). The positive onset potential of the FTO|CuBi₂O₄ electrode indicates a more positive flat-band or valence band edge potential of FTO|CuBi₂O₄, in agreement with previous reports in the literature.^{23,24} Mott-Schottky plot analysis resulted in a flat-band potential of CuO and CuBi₂O₄ of 0.69 ± 0.01 V and 0.81 ± 0.03 V vs. NHE in neutral aqueous electrolyte solution (Fig. S5, ESI†), respectively, which is in agreement with the onset potentials in the LSV measurements.

PEC experiments with the FTO|CuO, FTO|CuBi₂O₄ and FTO|CuO|CuBi₂O₄ heterojunction electrodes in acetonitrile solution in the presence of an electron acceptor, ethyl viologen dication (EV²⁺), were subsequently performed to avoid photodegradation in water with the bare metal oxide electrodes (Fig. S6 and S7, ESI†).^{6,24,30} The photocurrent measured under these conditions did not contain any background current from electrode photodecomposition and was therefore smaller than in the aqueous solution. Consequently, the FTO|CuO and FTO|CuBi₂O₄ electrodes show stable photocurrent without noticeable photodegradation in acetonitrile solution (Fig. S7, ESI†). The steady-state photocurrent measured by CA was only approximately 30% of the transient photocurrent for all electrodes measured by LSV and the large transient behavior, including peak-shaped photocurrent response in the LSV, indicates significant surface recombination at the photocathodes and visible light absorption by EV⁺ formed at the electrode surface.³¹ Investigation of systematic surface passivation would be an efficient method to further reduce the recombination rate at surface defects and leading to an enhanced photocurrent.

The effect of different amounts of the Cu-based semiconductors deposited on FTO on the photocurrent was also studied in acetonitrile with EV²⁺ for each electrode (Fig. S7, ESI†). The optimized amount of metal ions was 2.2, 0.45, and 2.2|0.45 μmol cm⁻² for

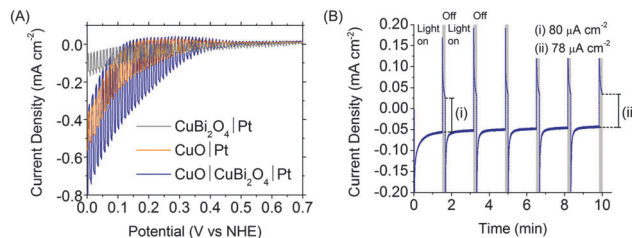


Fig. 2 (A) Photocurrent response of FTO|CuO|Pt, FTO|CuBi₂O₄|Pt and FTO|CuO|CuBi₂O₄|Pt electrodes at a scan rate of 20 mV s⁻¹ under chopped visible light irradiation ($\lambda > 420$ nm) and (B) CA runs of FTO|CuO|CuBi₂O₄|Pt electrode under visible light irradiation for 10 min (pH 6.8, 0.3 M K₂SO₄, 0.1 M phosphate, deaerated). CA was measured with an applied potential of 0.2 V vs. NHE to the photocathodes.

CuO, CuBi₂O₄, and CuO|CuBi₂O₄, respectively, used for electrode preparations in further experiments (cross-section images and film thickness are shown in Fig. S2, ESI†). Thicker films resulted in a decreased photocurrent response or physical instability.

The CuO|CuBi₂O₄ heterojunction displayed a substantially higher photocurrent in LSV and CA measurements than the homo-layered FTO|CuO or FTO|CuBi₂O₄ electrodes (Fig. 2 and Fig. S6–S8, ESI†). For example, a three times higher photocurrent was obtained with the CuO|CuBi₂O₄ heterojunction for EV²⁺ reduction than with the homo-layered electrodes at -0.45 V vs. NHE (Fig. S7, ESI†).

The higher photocurrent results from better electron-hole separation in the CuO|CuBi₂O₄ heterojunction than in CuO or CuBi₂O₄ for the following reasons: the photocurrent at FTO|CuO or FTO|CuBi₂O₄ was not limited by light absorption (thickness dependence in Fig. S7D, ESI†) and not hindered by the reaction kinetics for EV²⁺ reduction.³⁰ The gradual increase of photocurrent observed at the CuO|CuBi₂O₄ heterojunction during CA can be assigned to structural changes at the CuO and CuBi₂O₄ interface (Fig. S7C and S9, ESI†).³²

The Pt electrocatalyst was then photo-deposited on the electrodes from a K₂PtCl₄ solution (see ESI† and Fig. S10) in order to enhance the activity and stability of the photocathodes in aqueous electrolyte solution during illumination.^{33–35}

LSV scans for FTO|CuBi₂O₄|Pt, FTO|CuO|Pt and FTO|CuO|CuBi₂O₄|Pt measured in pH 6.8 aqueous solution are shown in Fig. S8 (UV-vis irradiation, ESI†) and Fig. 2 ($\lambda > 420$ nm). Photocurrents at FTO|CuO|CuBi₂O₄|Pt were more than twice as high as at FTO|CuO|Pt and FTO|CuBi₂O₄|Pt. In addition, the Pt-modified electrodes exhibited a small improvement in photostability compared to the Pt-free electrodes and reduced photodegradation was observed after 10 min irradiation in the aqueous solution (Fig. 2 and Fig. S11, ESI†). A steady-state photocurrent of 100 and 80 μA cm⁻² was observed during CA for the FTO|CuO|CuBi₂O₄|Pt electrode under UV-vis and visible light ($\lambda > 420$ nm) irradiation, respectively. Thus, approximately 80% of the photocurrent is generated by $\lambda > 420$ nm light absorption at the heterojunction electrode (Fig. 3). However, photocurrents with FTO|CuO|CuBi₂O₄|Pt do still not display long term stability and currents started to decrease quickly after approximately 10 min, with approximately 60% of the photocurrent



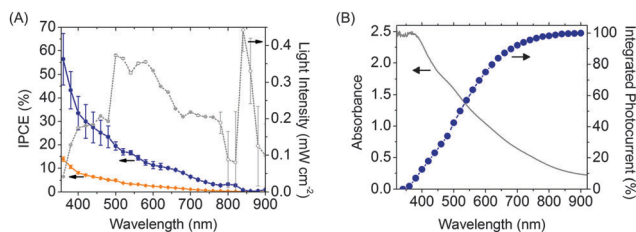


Fig. 3 (A) IPCE plots at 0 (blue) and 0.2 V vs. NHE (orange) and light intensity (grey) at different wavelengths. (B) UV-vis absorption spectrum (solid line) and integrated photocurrent over the wavelength based on IPCE from (A) at 0 V (blue circles) of CuO|CuBi₂O₄|Pt in a deaerated aqueous solution (0.3 M K₂SO₄, pH 6.8, 0.1 M phosphate).

remaining after 20 min (Fig. S11D, ESI†). The photo-instability of FTO|CuO|CuBi₂O₄|Pt originates presumably from non-conformal coating of the electrocatalyst on the photocathode and the resulting lack of complete protection from the electrolyte solution (Fig. S10, ESI†).^{19,36,37} LSV scans also indicate a non-negligible dark current with FTO|CuO|CuBi₂O₄|Pt and FTO|CuO|Pt electrodes (Fig. 2A), which indicates possible reduction of the photocathodes. Studies to ensure longer time stability of the photocathodes with conformal and noble-metal free coatings in aqueous solution are currently in progress in our laboratory.

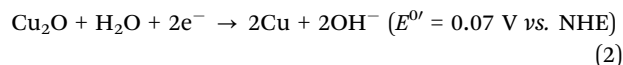
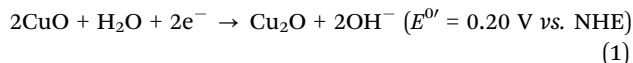
Mott–Schottky plots of FTO|CuO and FTO|CuBi₂O₄ allowed us to determine the flat-band potentials of the heterojunction, which is closely placed to the valence band edge for a heavily p-doped semiconductor such as CuO and CuBi₂O₄ (see above). The size of the band gap, or position of conduction band-edge of CuO and CuBi₂O₄ could not be unambiguously determined by UV-vis absorption spectroscopy and Tauc plots (Fig. S12, ESI†) and is not precisely known from the literature.^{22–24,38} CuO was reported with a wide range of indirect band gap of 1.2 to 1.9 eV^{24,38} and CuBi₂O₄ with a band gap between 1.5 to 1.8 eV.^{23,39} We expect the band-gap size to be larger than 1.2 eV for CuO and greater than 1.3 eV for CuBi₂O₄ based on the observed photoreduction of EV²⁺ and proton reduction reactions both at the FTO|CuO and FTO|CuBi₂O₄ electrodes as shown in Fig. 2 and Fig. S6 (ESI†).

The valence band offsets or internal electric field given in the heterojunction indicates that enhanced electron–hole separation can occur in the heterostructured electrode of CuO and CuBi₂O₄. The heterojunction of FTO|CuO|CuBi₂O₄|Pt generates at least twice the photocurrent of homo-layered FTO|CuO|Pt or FTO|CuBi₂O₄|Pt electrodes due to the reduction of electron–hole recombination by the band offsets provided in the heterostructure. In contrast, a deteriorating effect was observed with an inverted heterojunction, *i.e.*, FTO|CuBi₂O₄|CuO. With this electrode, a reduced photocurrent results from the deep valence band of CuBi₂O₄ and the resulting trapping of holes and increased electron–hole recombination at the interfaces between the CuBi₂O₄ and CuO layers (Fig. S13, ESI†).

H₂ generation at the photocathodes was confirmed by electrochemical detection of H₂ (Fig. S14, ESI†): a Pt ultramicroelectrode (UME) with a diameter of 100 μm with an applied potential of –0.3 V for H₂ oxidation was placed near (at an estimated distance

of approximately 500 μm) the FTO|CuO|CuBi₂O₄|Pt electrode to detect H₂ during back-side irradiation of the photocathode (see Experimental section in ESI† for details). Thereby, H₂ diffuses from the photoelectrode to the Pt UME and the H₂ oxidation current at the latter is proportional to the H₂ evolved at the former electrode. Note that the FTO|CuO|CuBi₂O₄|Pt electrode has a small electrode area and was largely covered by an insulating epoxy resin resulting in a small current in Fig. S14 (ESI†). A H₂ oxidation current was observed at the Pt UME upon irradiation of the FTO|CuO|CuBi₂O₄|Pt electrode. The electrooxidation current at Pt demonstrates H₂ evolution at the photocathode.

The electrocatalyst Pt on the heterojunction facilitates the reaction kinetics for HER and fewer photoexcited electrons are consumed for the electrode decomposition reactions shown in eqn (1) and (2) at pH 6.8.¹³ We note that H₂ was only detected at the Pt UME with the FTO|CuO|CuBi₂O₄|Pt photocathode, but not at FTO|CuO|CuBi₂O₄ without Pt, where the photocurrents are mainly due to photodecomposition of the heterojunction electrode.^{11,13,19,36,40} Previously, photoelectrodeposition of electrocatalyst layers, *e.g.* Ru and Pt onto p-WSe₂ for HER¹⁹ or Co–Pi on Ba-doped Ta₃N₅ for OER,³³ were used to fabricate the protective layers to reduce the photodecomposition reactions and to utilize electrons and holes primarily for HER and OER.



Incident photon to current conversion efficiencies (IPCE) of FTO|CuO|CuBi₂O₄|Pt with UV-vis absorption spectra shown in Fig. 3 indicate an excellent visible light response of the heterojunction electrode (see ESI† for details). The heterojunction electrode shows a maximum IPCE of 60% at 0 V for high-energy photon absorption, and shows a visible response at the wavelength up to 850 nm. The effective band-gap size of FTO|CuO|CuBi₂O₄|Pt electrode is therefore approximately 1.5 eV based on IPCE measurements. In addition, integration of the photocurrent over the wavelength from the IPCE measurements in Fig. 3A further confirmed the efficient visible light harvesting of the heterojunction electrode (Fig. 3B). Fig. 3B shows the wavelength dependent photocurrent produced by absorbed photons. More than 80% of the photocurrent was generated by visible light irradiation with wavelength longer than 420 nm. The visible light response of the heterojunction in LSVs is also shown in Fig. S15 (ESI†). IPCE values at various applied potentials in Fig. S16 (ESI†) show that the photoactivity enhancement in the heterojunction electrode appeared under monochromatic irradiation agrees well with the visible light response in Fig. 2. Note that the beam intensities used for IPCE measurements indicated in Fig. 3A were different from the AM 1.5 irradiance, which can affect IPCE values.⁴¹

In summary, a CuO|CuBi₂O₄|Pt electrode for visible light driven H₂ evolution in aqueous electrolyte solution is reported. The novel heterojunction electrode structure reduces charge recombination, has a narrow band-gap of approximately 1.5 eV



and can be stabilized in water with a suitable electrocatalyst layer. CuO|CuBi₂O₄ is also easy to assemble, does not contain prohibitively expensive materials and is therefore a promising candidate for visible absorption and charge-separation in solar-to-fuel conversion devices with theoretical efficiencies of more than 20%.^{2,3} CuO and CuBi₂O₄ form an excellent heterojunction pair, which more than doubles the photoactivity compared to the corresponding monolayer electrodes. Work to further increase the performance and stability of photoelectrodes in aqueous solution and replacement of Pt by inexpensive electrocatalysts is currently in progress in our laboratory.

Acknowledgements

This work was supported by the Christian Doppler Research Association (Austrian Federal Ministry of Science, Research and Economy and the National Foundation for Research, Technology and Development), the OMV Group, the EPSRC (EP/H00338X/2) and BBSRC (BB/K010220/1).

Notes and references

- 1 A. Fujishima and K. Honda, *Nature*, 1972, **238**, 37–38.
- 2 M. C. Hanna and A. J. Nozik, *J. Appl. Phys.*, 2006, **100**, 074510.
- 3 M. F. Weber and M. J. Dignam, *Int. J. Hydrogen Energy*, 1986, **11**, 225–232.
- 4 J. Brillet, J.-H. Yum, M. Cornuz, T. Hisatomi, R. Solarska, J. Augustynski, M. Graetzel and K. Sivula, *Nat. Photonics*, 2012, **6**, 824–828.
- 5 O. Khaselev and J. A. Turner, *Science*, 1998, **280**, 425–427.
- 6 A. J. Bard and M. S. Wrighton, *J. Electrochem. Soc.*, 1977, **124**, 1706–1710.
- 7 C. Yang, Z. Wang, T. Lin, H. Yin, X. Lu, D. Wan, T. Xu, C. Zheng, J. Lin, F. Huang, X. Xie and M. Jiang, *J. Am. Chem. Soc.*, 2013, **135**, 17831–17838.
- 8 K. Sivula, R. Zboril, F. Le Formal, R. Robert, A. Weidenkaff, J. Tucek, J. Frydrych and M. Grätzel, *J. Am. Chem. Soc.*, 2010, **132**, 7436–7444.
- 9 H. S. Park, K. C. Leonard and A. J. Bard, *J. Phys. Chem. C*, 2013, **117**, 12093–12102.
- 10 J. A. Seabold and K.-S. Choi, *Chem. Mater.*, 2011, **23**, 1105–1112.
- 11 Y.-H. Lai, T. C. King, D. S. Wright and E. Reisner, *Chem. – Eur. J.*, 2013, **19**, 12943–12947.
- 12 E. L. Warren, J. R. McKone, H. A. Atwater, H. B. Gray and N. S. Lewis, *Energy Environ. Sci.*, 2012, **5**, 9653–9661.
- 13 A. Paracchino, V. Laporte, K. Sivula, M. Gratzel and E. Thimsen, *Nat. Mater.*, 2011, **10**, 456–461.
- 14 M. Hara, T. Kondo, M. Komoda, S. Ikeda, K. Shinohara, A. Tanaka, J. N. Kondo and K. Domen, *Chem. Commun.*, 1998, 357–358.
- 15 C.-Y. Lin, Y.-H. Lai, D. Mersch and E. Reisner, *Chem. Sci.*, 2012, **3**, 3482–3487.
- 16 M. H. Lee, K. Takei, J. Zhang, R. Kapadia, M. Zheng, Y.-Z. Chen, J. Nah, T. S. Matthews, Y.-L. Chueh, J. W. Ager and A. Javey, *Angew. Chem., Int. Ed.*, 2012, **51**, 10760–10764.
- 17 D. Yokoyama, T. Minegishi, K. Jimbo, T. Hisatomi, G. Ma, M. Katayama, J. Kubota, H. Katagiri and K. Domen, *Appl. Phys. Express*, 2010, **3**, 101202.
- 18 T. J. Jacobsson, V. Fjallstrom, M. Sahlberg, M. Edoff and T. Edvinsson, *Energy Environ. Sci.*, 2013, **6**, 3676–3683.
- 19 J. R. McKone, A. P. Pieterick, H. B. Gray and N. S. Lewis, *J. Am. Chem. Soc.*, 2013, **135**, 223–231.
- 20 J. Gu, Y. Yan, J. W. Krizan, Q. D. Gibson, Z. M. Detweiler, R. J. Cava and A. B. Bocarsly, *J. Am. Chem. Soc.*, 2014, **136**, 830–833.
- 21 A. Kargar, Y. Jing, S. J. Kim, C. T. Riley, X. Pan and D. Wang, *ACS Nano*, 2013, **7**, 11112–11120.
- 22 T. Arai, Y. Konishi, Y. Iwasaki, H. Sugihara and K. Sayama, *J. Comb. Chem.*, 2007, **9**, 574–581.
- 23 N. T. Hahn, V. C. Holmberg, B. A. Korgel and C. B. Mullins, *J. Phys. Chem. C*, 2012, **116**, 6459–6466.
- 24 S. P. Berglund, H. C. Lee, P. D. Núñez, A. J. Bard and C. B. Mullins, *Phys. Chem. Chem. Phys.*, 2013, **15**, 4554–4565.
- 25 C. Henmi, *Mineral. Mag.*, 1995, **59**, 545–548.
- 26 J. Bandara, I. Guasaquillo, P. Bowen, L. Soare, W. F. Jardim and J. Kiwi, *Langmuir*, 2005, **21**, 8554–8559.
- 27 Z. Zhang and P. Wang, *J. Mater. Chem.*, 2012, **22**, 2456–2464.
- 28 D. Praveen Kumar, M. V. Shankar, M. Mamatha Kumari, G. Sadanandam, B. Srinivas and V. Durgakumari, *Chem. Commun.*, 2013, **49**, 9443–9445.
- 29 A. Radi, D. Pradhan, Y. Sohn and K. T. Leung, *ACS Nano*, 2010, **4**, 1553–1560.
- 30 H. Ye, H. S. Park, V. A. Akhavan, B. W. Goodfellow, M. G. Panthani, B. A. Korgel and A. J. Bard, *J. Phys. Chem. C*, 2011, **115**, 234–240.
- 31 L. M. Peter, *Chem. Rev.*, 1990, **90**, 753–769.
- 32 I. Hwang, C. R. McNeill and N. C. Greenham, *J. Appl. Phys.*, 2009, **106**, 094506.
- 33 Y. Li, L. Zhang, A. Torres-Pardo, J. M. González-Calbet, Y. Ma, P. Oleynikov, O. Terasaki, S. Asahina, M. Shima, D. Cha, L. Zhao, K. Takanabe, J. Kubota and K. Domen, *Nat. Commun.*, 2013, **4**, 2566.
- 34 E. M. P. Steinmiller and K.-S. Choi, *Proc. Natl. Acad. Sci. U. S. A.*, 2009, **106**, 20633–20636.
- 35 B. Kraeutler and A. J. Bard, *J. Am. Chem. Soc.*, 1978, **100**, 4317–4318.
- 36 C. G. Morales-Guio, S. D. Tilley, H. Vrubel, M. Gratzel and X. Hu, *Nat. Commun.*, 2014, **5**, 3059.
- 37 B. Seger, A. B. Laursen, P. C. K. Vesborg, T. Pedersen, O. Hansen, S. Dahl and I. Chorkendorff, *Angew. Chem., Int. Ed.*, 2012, **51**, 9128–9131.
- 38 D. Wu, Q. Zhang and M. Tao, *Phys. Rev. B*, 2006, **73**, 235206.
- 39 T. Arai, M. Yanagida, Y. Konishi, Y. Iwasaki, H. Sugihara and K. Sayama, *J. Phys. Chem. C*, 2007, **111**, 7574–7577.
- 40 S. Y. Reece, J. A. Hamel, K. Sung, T. D. Jarvi, A. J. Esswein, J. J. H. Pijpers and D. G. Nocera, *Science*, 2011, **334**, 645–648.
- 41 Y. Nosaka and M. A. Fox, *J. Phys. Chem.*, 1986, **90**, 6521–6522.

